



Norwegian
Meteorological
Institute

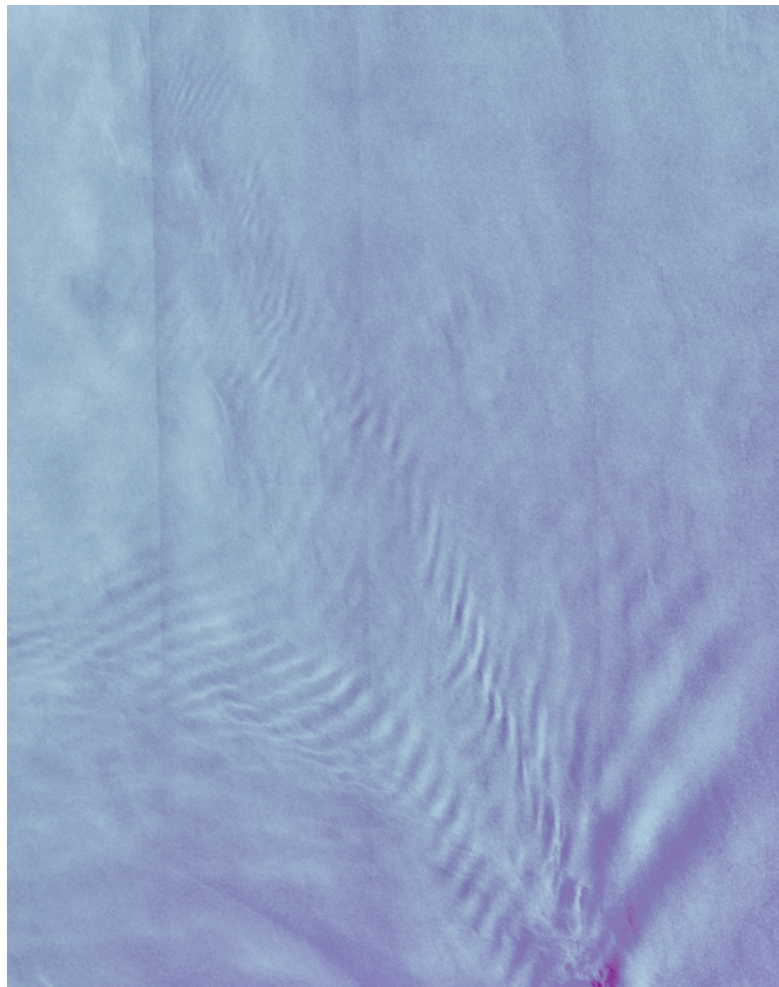
METreport

No. 15/2024
ISSN 2387-4201
Meteorology

Evaluation of SAR wind

Comparison of Wind Speeds from MEPS and Arome Arctic with SAR Open
Wind Data

Tomine Stenheim Øyen, Eirik Mikal Samuelsen, Morten Wergeland Hansen





Norwegian
Meteorological
Institute

METreport

Title Evaluation of SAR wind - Comparison of Wind Speeds from MEPS and Arome Arctic with SAR Open Wind Data	Date May 14, 2025
Section Meteorology	Report no. 15/2024
Authors Tomine Stenheim Øyen, Eirik Mikal Samuelsen, Morten Wergeland Hansen	Classification <input checked="" type="radio"/> Free <input type="radio"/> Restricted
Client Norwegian Research Council	Client's reference 'Multidisciplinary approach for spray icing modelling and decision support in the Norwegian maritime sector' (SPRICE). Grant Number 320843 at NFR, and MET Norway project number is 281570.
Keywords Synthetic Aperture Radar (SAR), Wind, Open ocean verification, Harmonie AROME	

Disciplinary signature

Responsible signature

Abstract

This study evaluates the performance of two high-resolution Numerical Weather Prediction (NWP) models, MEPS and AROME-Arctic, against Synthetic Aperture Radar (SAR)-derived wind fields in Arctic regions from May to October 2024. The research focuses on verifying simulated 10-m wind speed under various sea surface conditions, coastal dynamics, and during convective weather events. Results highlight that while both models predict moderate wind regimes reasonably accurate, systematic underestimations occur in rough sea states and convective environments. SAR data, though valuable for small-scale verification, show limitations due to ambiguities in ice-affected areas. Findings underline the importance of refining NWP model parameterization and horizontal resolution in order to increase the forecast accuracy in high-latitude. In addition, it would be advantageous to modify the SAR wind retrieval algorithms further, in order to improve high-quality wind-observation availability in this otherwise observation-sparse region.

Contents

1	Introduction	5
2	Data and Methodology	7
2.1	NWP Models	7
2.2	Satellite Data	8
2.3	Sentinel-1A Data Collocation with NWP Models	8
2.4	Outlier Detection and Removal	9
2.5	Verification Metrics	9
3	Results	11
3.1	Distinguishing Sea-Ice Drift from SAR-Derived Wind Speeds	11
3.2	Wind Speed Prediction during Varied Sea Surface Conditions	15
3.3	Wind Speed Variability Across Coastal and Open Ocean Regions	19
3.4	Wind Discrepancies in Convective Environments	24
4	Discussion	30
5	Conclusions	33

1 Introduction

Accurate and reliable weather predictions in the Arctic have become increasingly important due to the recent uptick in human activities like shipping, tourism, and resource extraction in the region. Although numerical weather prediction (NWP) models have improved considerably in recent decades, particularly in the Arctic (Jung and Leutbecher, 2007), the region still poses challenges for these models due to the sparse observational network, small spatial scales of Arctic weather phenomena such as polar lows, and the focus of these models on mid- and lower-latitude weather (Køltzow et al. (2021), Jung and Matsueda (2016)). Additionally, the sparse distribution of in-situ measurements impedes the effective initialization and validation of NWP models, leading to increased uncertainty in forecasts. The use of remote sensing observations, such as synthetic aperture radar (SAR), has the potential to improve the validation and development of these models in high-latitude regions, such as the Arctic (Tollinger and Graversen, 2024). Observations from SAR can provide additional knowledge of the spatial and temporal variability of atmospheric conditions over the Arctic, due to the high spatial resolution, large-scale coverage, and ability to provide measurements even in cloudy conditions or during polar night. SAR-wind products are able to estimate ocean surface wind speeds on a much finer scale than regional operational NWP models, which can help provide insights into small-scale weather phenomena that are often not accurately resolved. It is, however, important to note that SAR-derived wind fields are not ground truth, as they rely on empirical geophysical model functions (GMF) to retrieve wind speed from the radar backscatter signal. The ambiguities involved in SAR wind retrieval algorithms, lack of in situ validation, and potential inaccuracies in the NWP wind direction information used as input for the retrieval, may all introduce uncertainties in the resulting wind-field estimations. Currently, wind speeds derived from SAR through GMFs are only valid up to about 20 – 25 m s^{-1} (Hersbach et al. (2007), Stoffelen et al. (2017)), which limits their usefulness for more extreme wind conditions. Recent studies have developed techniques for estimating wind fields from SAR imagery without relying on external wind direction inputs, potentially enhancing numerical forecasting of weather systems featuring strong wind gradients, such as polar lows (Tollinger et al., 2021).

This study aims to verify the performance of two high-resolution, operational NWP models against SAR-derived wind fields from the beginning of May 2024 to the end of October

2024, focusing on the simulated 10-m wind speed. Additionally, possible limitations and uncertainties in both the NWP models and the SAR wind retrieval are discussed.

The two NWP models and the remote sensing observations used in this study are briefly described in Section 2, along with the methodology used for collocation and wind retrieval. The results of the model verification are presented in Section 3 including three separate cases focusing on the performance of the models during different wind regimes. In Section 3.4, two cases describing separate convective events are investigated where examples of discrepancies between the two NWP model predictions are observed. Lastly, Section 4 provides a discussion of the limitations and uncertainties in the analysis, as well as considerations for future work.

2 Data and Methodology

2.1 NWP Models

The NWP models evaluated in this study include the Nordic convection-permitting MEPS system (Bengtsson et al., 2017), operating with a 2.5-km grid resolution (HARMONIE-AROME configuration; HIRLAM-ALADIN Research on Mesoscale Operational NWP in Europe), and the operational European Arctic regional model AROME-Arctic (Müller et al., 2017), with the same 2.5-km grid spacing. Both systems are designed with 65 vertical levels and are based on a shared core model configuration. However, they differ in domain coverage (Figure 1), lateral boundary forcing, and certain parametrization schemes. Operational forecasts are generated eight times a day using six-hourly boundary conditions derived from the ECMWF IFS-HRES global system.

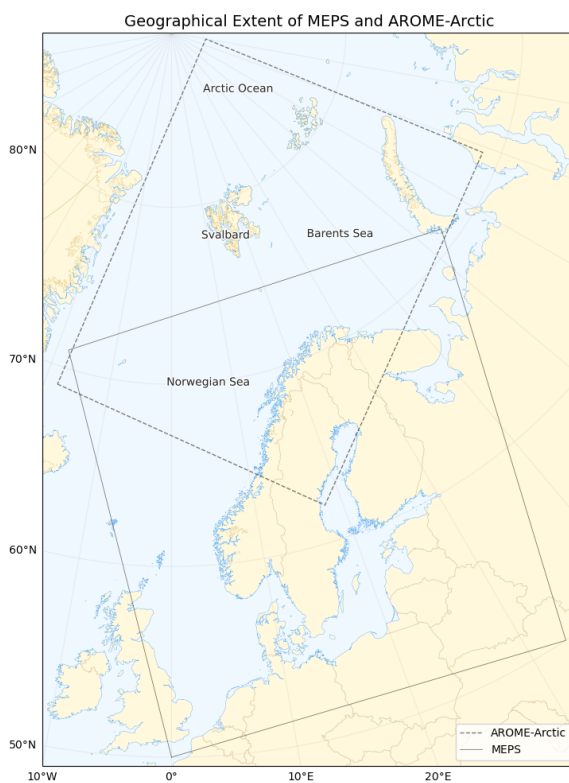


Figure 1: Geographical extent of the Nordic MEPS (solid black line) and AROME-Arctic (dashed line) model domains. The map illustrates the coverage areas of the convection-permitting NWP systems, including key regions such as the Arctic Ocean, Barents Sea, Norwegian Sea, and Svalbard.

2.2 Satellite Data

Sentinel-1A

SAR images are sourced from the Sentinel-1A satellite operating in the C-band frequency range. The SAR data utilized are Level-1 Ground Range Detected (GRD) products, acquired in dual-polarization mode, including vertical (VV+VH) and horizontal (HH+HV) polarizations. The images are acquired in two specific modes: Interferometric Wide Swath (IW), which offers a swath width of 250 km and is primarily used for coastal regions, and Extra Wide Swath (EW) mode, with a 400 km swath, mainly used in polar arctic areas.

Wind Speed Estimations

The wind-speed estimation follows the typical steps as described in [Hersbach et al. \(2007\)](#) and [Stoffelen et al. \(2017\)](#). The CMOD5.N model function provides an empirical relationship relating the normalized radar cross-section measurement from the SAR sensor, the radar incidence angle, and the (neutral) ocean wind speed and direction at 10-m height (10-m neutral wind). Since the SAR wind direction is not available, the modelled wind direction from the AROME-Arctic and the control member of MEPS NWP systems are used as input for the CMOD5.N model to derive the SAR wind speed.

2.3 Sentinel-1A Data Collocation with NWP Models

The map-projected sea-surface wind fields estimated from Sentinel-1A SAR data and collocated with the 10-m wind fields from the MEPS and AROME-Arctic NWP models can be sourced from the Norwegian Meteorological Institute's (MET Norway) THREDDS Data Server. It is important to note that, the datasets obtained from the THREDDS Data Server are the direct output from the model without any detailed post-processed model output with bias correction.

Given that the acquisition times of the SAR scenes and the NWP model forecasts do not always coincide, i.e. the NWP model output is every hour, a temporal matching within a 30-minute time window is performed during the collocation process to account for temporal discrepancies. In addition, the initial time of the model closest to the SAR scene is applied, meaning that there are only short term forecasts of maximum 3 hours applied in the study. The extent covered by the SAR swath is used as the common domain and the model output is remapped to this grid using nearest-neighbour interpolation.

2.4 Outlier Detection and Removal

During the initial data analysis, several SAR-derived wind speed estimates are found to be significantly higher than both neighbouring data points and corresponding values from NWP models. These anomalous readings can often result from factors such as radar calibration errors, distortions due to sea ice, or contamination from nearby land surfaces or vessels. In order to mitigate the influence of such outliers, an outlier detection and removal process is implemented. This process involves categorizing wind speed values based on their deviation from the median of surrounding grid points. A threshold is established to identify and exclude outliers, ensuring that only data points within a specified range of the median are retained. The Median Absolute Deviation (MAD) (Huber, 2004) is employed as a measure of statistical dispersion, and the deviation of each data point from the median is calculated using the following formula:

$$M_i = \frac{0.6745(x_i - \tilde{x}_i)}{\text{MAD}},$$

where x_i represents the individual data point, \tilde{x}_i denotes the median of the dataset, and MAD is the Median Absolute Deviation:

$$b \text{ MAD} = b \text{ median}\{|x_i - \tilde{x}_i|\},$$

where $b = 1.4826$, which is the scaling factor for Gaussian distributions, such that the constant 0.6745 is used to scale the MAD to be consistent with the standard deviation for a normal distribution (Rousseeuw and Croux, 1993).

2.5 Verification Metrics

The statistical performance of the models is evaluated against SAR using the following key metrics:

1. Median **Bias**, which calculates the median of the difference between the predicted (model) wind speed and the observed (SAR) wind speed, serving as an indicator of systematic over- or underestimation by the models. Median bias is chosen for robustness, as it is less sensitive to outliers than the mean.
2. Median absolute error or **MAE**, which quantifies the absolute deviations between observed and modelled wind speeds, offering a direct measure of prediction accuracy. Median absolute error instead of the more typical mean absolute error is

here applied to ensure that extreme values do not disproportionately affect the error estimation, particularly during variable wind conditions.

3. Spearman's Rank Correlation Coefficient, which is a non-parametric correlation assesses the strength and direction of monotonic relationships between observed and modelled wind speeds, independent of linear assumptions. Spearman's correlation is transformed using Fisher's Z-transformation for aggregation, as this approach stabilizes the variance and allows for meaningful averaging across samples. Inverse transformation is then applied to obtain the final correlation values for interpretation.

3 Results

3.1 Distinguishing Sea-Ice Drift from SAR-Derived Wind Speeds

Impact of Sea-Ice on SAR Wind Retrieval

Sea ice evolves through various stages: from open water to new ice, young ice, first-year ice, and eventually multiyear ice. Throughout these transitions, there are changes in surface roughness and salinity, leading to variations in radar backscatter intensity (Onstott, 1992). SAR leverages these backscatter variations to distinguish between different ice types based on their age and physical characteristics. However, the sensitivity of SAR backscatter to these ice properties introduces ambiguities in wind retrieval processes. In particular, sea ice-covered regions have been known to exhibit backscatter signatures similar to those of open water under high wind conditions, causing SAR wind-retrieval to erroneously interpret these areas as experiencing high wind speeds (Horstmann et al., 2000).

In each SAR resolution cell, the backscatter values are influenced by multiple ice parameters, including the stage of ice development, unresolved ice forms within the imagery, surface characteristics of ice and snow, and overall surface roughness. These factors contribute to significant ambiguities in interpreting SAR backscatter data. For instance, a strong backscatter signal may originate from various ice conditions such as hummocked thick first-year ice, thin ice with frost flowers, or areas with packed ice cakes and small floes. Moreover, the backscatter from open water surfaces varies significantly with wind speed and direction, leading to increased backscatter at higher wind speeds. Figure 2 shows how the SAR backscatter (in dB) varies over the different stages of sea ice evolution, along with the backscatter variation over open water with increasing surface roughness.

The inherent variability of sea-ice surfaces poses challenges for both SAR wind retrieval and NWP model simulations. In regions with extensive sea-ice coverage, discrepancies between SAR-derived and model wind fields are likely to increase due to the differing methodologies by which each system interprets wind information. Specifically, SAR may produce false positives in wind speed estimations where the backscatter from rough ice mimics that of open water under high wind conditions.

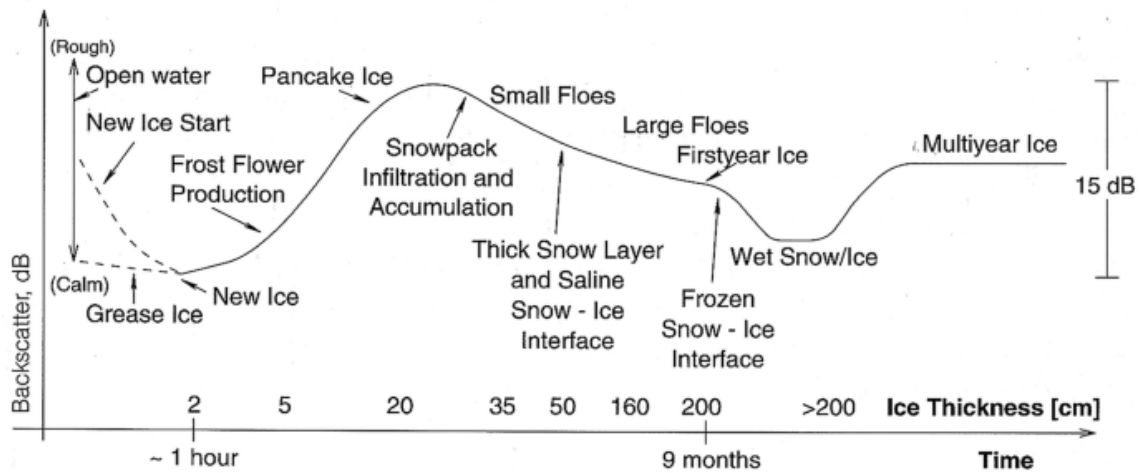


Figure 2: SAR backscatter (dB) as a function of sea ice thickness (cm) and time, highlighting different stages of ice formation and transformation, including open water, new ice, frost flower production, and the development of multiyear ice. (Adopted from Johannessen (2020))

The SAR-derived wind field in Figure 3, from 2 July 2024, exemplifies a typical case where drift ice significantly influences SAR wind observations. Although the observed wind speeds, ranging from 0.5 to 25 m s^{-1} , fall within plausible wind speeds ranges, the presence of sharp gradients and the formation of cyclonic eddies within the wind field suggest that these features are predominantly influenced by the drift ice dynamics rather than actual atmospheric wind patterns.

The purpose of the following section is to illustrate the potential inaccuracies in using Sentinel-1A EW mode GRD SAR products with HH+HV polarization for operational wind field derivation in polar Arctic regions, especially when integrating with NWP models. The observed ambiguities arising from sea-ice dynamics emphasizes the necessity for cautious interpretation of SAR data. Without effectively distinguishing between ice-induced and wind-induced signals, the integration of SAR products with NWP models may result in erroneous wind-field representations. Thus, its use in operational wind-field verification should be treated with caution and supplemented by other observational data sources to validate NWP-model performance in these regions.

SAR and NWP Wind Speed Differences in the Arctic

In order to illustrate how sea-ice conditions can impact the agreement between SAR-derived and NWP-simulated wind fields, a brief visual comparison is provided for wind fields derived on 1 October 2024. Figure 4 shows how each data source estimates the

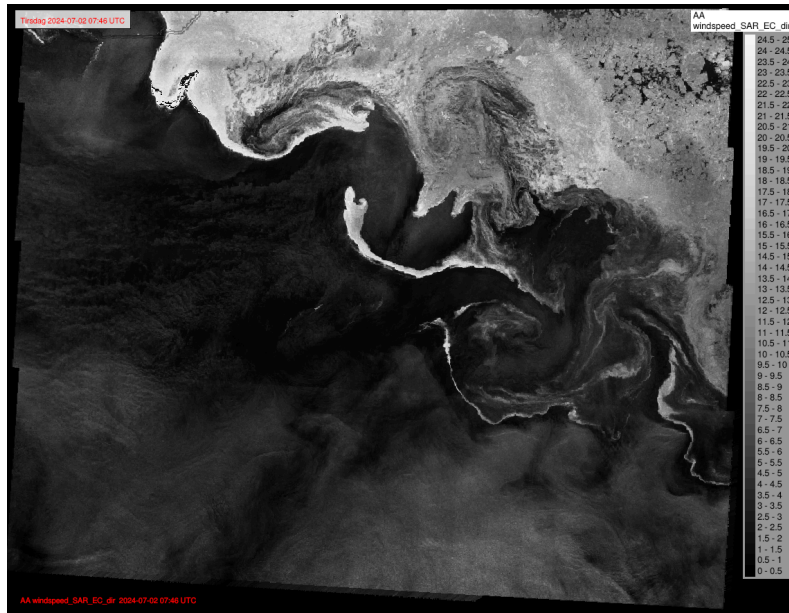


Figure 3: SAR-derived wind field captured on 2 July 2024, at 07:46:36 UTC using EW swath mode and HH+HV polarization. The image shows wind speed variations across the ice-covered and open water regions, with wind speeds ranging from 0.5 to 25 m s^{-1} .

wind conditions north of Svalbard on the provided date. The northern section of the image corresponds to consolidated sea ice, which appears as high-brightness regions. These regions are erroneously represented as high wind speeds (ranging from 20 to 38 m s^{-1}) by the SAR wind retrieval algorithm, despite the lack of actual high winds in this area.

In order to illustrate how sea-ice conditions may impact the agreement between SAR-derived and NWP-simulated wind fields, a brief visual comparison is provided for wind fields derived on 1 October 2024. Figure 4 shows how each data source estimates the wind conditions north of Svalbard on the given date. The northern section of the image depicts a clear high-brightness region, with wind speeds ranging from 20 m s^{-1} to 38 m s^{-1} . The open water regions in the southern portion of the image display more moderate backscatter values which correspond to relatively lower wind speeds ($< 15 \text{ m s}^{-1}$). Inspecting the sea-ice concentration outputs from AROME-Arctic (not shown) and sea-ice charts obtained from the MET Norway Ice Service, it is evident that the high wind speed signals detected by SAR in the northern region are mainly influenced by the presence of sea ice, rather than actual high wind speeds. Additionally, the AROME-Arctic model wind speeds in this region are significantly lower, ranging between 8 m s^{-1} and 14 m s^{-1} .

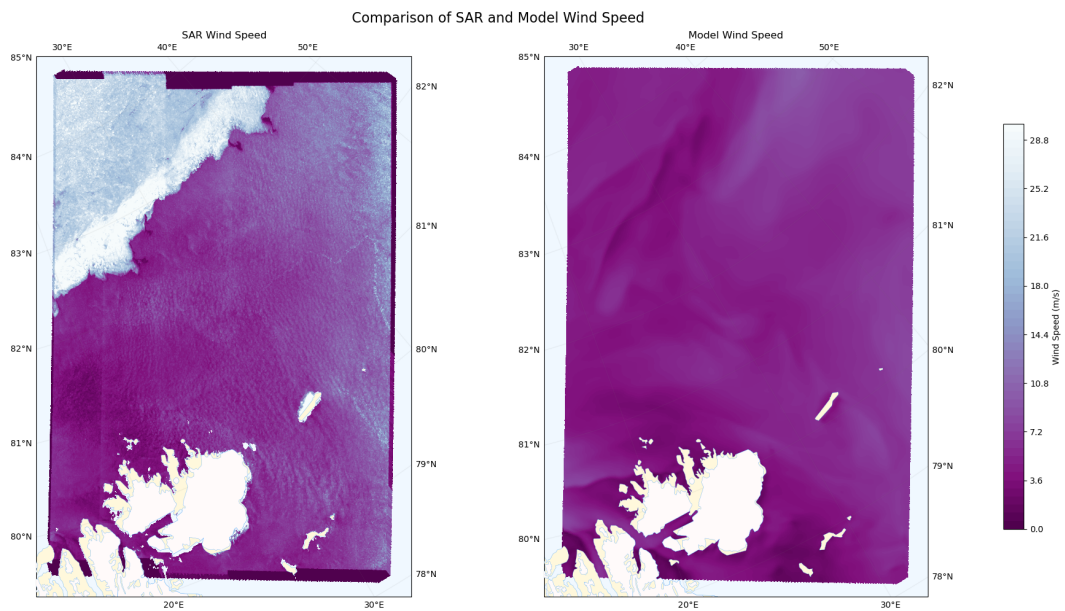


Figure 4: Comparison of SAR-derived wind speeds (left) and NWP model wind speeds (right) over Nordaustlandet and the ocean area northeast of Svalbard. The SAR data demonstrate wind speed gradients influenced by sea-ice dynamics, while the model data reflect atmospheric conditions independent of ice-related backscatter. Wind speeds are measured in meters per second (m s^{-1}).

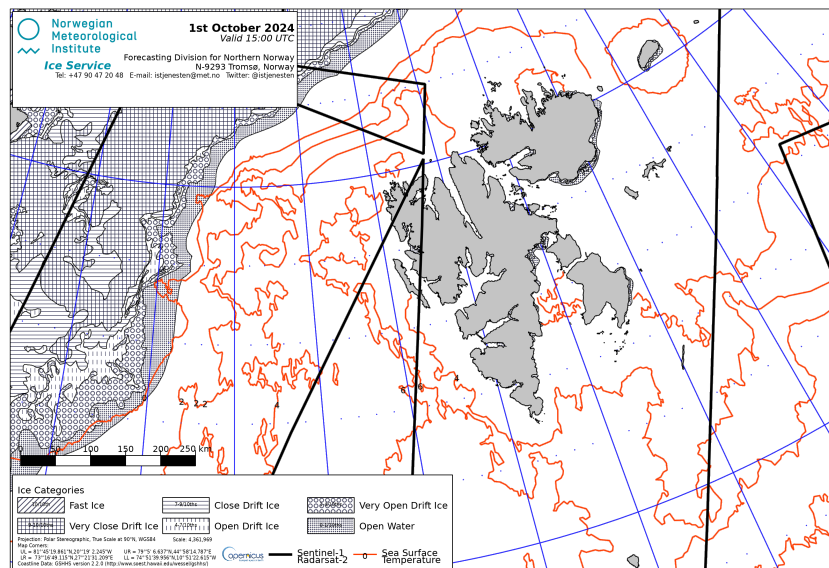


Figure 5: Ice chart from the Fram Strait region, valid on 1 October 2024 15:00 UTC. The chart provides an overview of sea-ice conditions for the time period and location where the SAR-derived wind field is acquired.

Over the open waters to the east, the SAR-derived wind speeds appear in a high degree to exceed those simulated by the numerical weather prediction model, and the realism of the SAR-wind in the EW mode is difficult to assess. Thus, in further analyses, SAR configurations using EW mode with HH+HV will be excluded, and only IW VV polarization imagery will be considered in verification.

3.2 Wind Speed Prediction during Varied Sea Surface Conditions

With the challenges posed by sea-ice backscatter ambiguities addressed, the remaining analysis will focus on the comparison of SAR-derived and NWP-modelled wind speeds in open water regions of the European Arctic. Rapidly changing surface conditions and varying wind regimes in high latitude regions is a well-known challenge for NWP models due to e.g. the complexity of air-sea interactions (Elvidge et al. (2016) and Wu et al. (2019)). In the Arctic, additional complexities, such as sea ice edge dynamics, polar lows, topographically induced flows due to high static stability, and increased sensitivity of the atmospheric boundary layer to surface conditions, exacerbate the variability in wind stress and surface fluxes. Existing bulk parametrizations for surface roughness often fail to account for the impact of wave dynamics, which can distort estimates of surface wind speed and fluxes, particularly during high-wind events or under rapidly evolving conditions. Coupled ocean-atmosphere NWP models and advanced parametrization schemes have been shown to improve model performance in these regions. However, limited observational data and computational constraints prevent further improvements, particularly for kilometre-scale, operational weather prediction models.

This section assesses the performance of AROME-Arctic and MEPS simulations in reproducing SAR-derived wind speeds during varied surface conditions, with a focus on capturing episodic high-wind events and validating the ability of the models to represent the dynamically complex near-surface wind field. Sea states are classified as calm ($< 5 \text{ m s}^{-1}$), moderate ($5 - 9 \text{ m s}^{-1}$), rough ($10 - 14 \text{ m s}^{-1}$), and very rough ($\geq 15 \text{ m s}^{-1}$). The analysis provides insights into systematic biases, spatial and temporal variability, and the accuracy of forecasts relative to SAR-derived wind fields. The results highlight differences in model performance across sea surface conditions and reveal how forecast accuracy varies with wind regime, surface roughness, and model framework.

Model Performance Across Sea States

Table 1 presents the performance metrics of the MEPS and AROME-Arctic NWP models in simulating wind speeds across different sea state conditions, and highlights the accuracy of the models and reliability in various wind regimes and surface roughness conditions from the beginning of May 2024 to the end of October 2024. A total of 238 cases are analysed with MEPS, and 230 cases are analysed with AROME-Arctic.

Table 1: Performance comparison of MEPS and AROME-Arctic models in simulating wind speeds across different sea state conditions. Metrics include Average Wind Speed (m/s), Average Bias (m/s), Average MAE (m/s), and Average Correlation Coefficient. Wind speeds leading to the corresponding sea states are categorized as Calm (< 5 m/s), Moderate ($5 - 9$ m/s), Rough ($10 - 14$ m/s), and Very Rough (≥ 15 m/s).

Model	Condition	Wind Speed (m s^{-1})	Average Bias (m s^{-1})	Average MAE (m s^{-1})	Average Corr
MEPS	Calm	< 5	0.73	1.55	0.15
	Moderate	$5 - 9$	-0.53	1.48	0.36
	Rough	$10 - 14$	-2.17	2.63	0.18
	Very Rough	≥ 15	-3.54	3.72	0.03
AROME-Arctic	Calm	< 5	0.91	1.61	0.16
	Moderate	$5 - 9$	-0.51	1.47	0.35
	Rough	$10 - 14$	-2.18	2.61	0.20
	Very Rough	≥ 15	-3.70	3.85	0.06

In calm conditions, both AROME-Arctic and MEPS tend to overestimate wind speeds, with average biases of 0.91 m s^{-1} and 0.73 m s^{-1} , respectively. The MAE is 1.61 m s^{-1} for AROME-Arctic and 1.55 m s^{-1} for MEPS, and both models have low correlation coefficients (0.16 and 0.15). As surface roughness increases, the models increasingly underestimate the wind speeds. Under moderate conditions, the average biases are -0.51 m s^{-1} for AROME-Arctic and -0.53 m s^{-1} for MEPS, with MAEs around 1.47 m s^{-1} and 1.48 m s^{-1} , respectively. The correlation coefficients peak under moderate conditions, reaching 0.35 for AROME-Arctic and 0.36 for MEPS. In rough conditions, the negative bias becomes more pronounced. AROME-Arctic shows an average bias of -2.18 m s^{-1} , and MAE of 2.61 m s^{-1} , and a correlation coefficient of 0.20. MEPS exhibits similar performance with an average bias of -2.17 m s^{-1} , an MAE of 2.63 m s^{-1} , and a correlation coefficient of 0.18. Under very rough conditions, both models show the largest underestimations, with biases reaching -3.70 m s^{-1} for AROME-Arctic and -3.54 m s^{-1} for MEPS. The MAEs increase to 3.85 m s^{-1} for AROME-Arctic and 3.72 m s^{-1} for MEPS, while the correlation coefficients drop to 0.06 and 0.03, respectively. Without comparing

the SAR wind product with observations it is difficult to assess whether these calculated model biases are exaggerated. However, the pattern with a positive bias for calm conditions and a negative bias for stronger wind conditions correspond to the findings from wind verification from oil and gas platform installations in the North Sea from the NORA3 reanalysis data set which also uses the Harmonie-AROME model with an almost similar horizontal grid spacing of 3 km (Solbrekke et al., 2021). In Solbrekke et al. (2021) the verification is performed at observation height instead of doing a correction of the observed wind values at instrument height down to 10 m which can lead to erroneous conclusions (Olsen et al., 2022). Similar verification is done in Kølitzow et al. (2024) which also shows an overall negative bias in MEPS when verified at sensor height. However, more comparison between observed winds and SAR-wind products must be performed in order to finally conclude whether the exact bias values calculated in this section are trustworthy.

Figure 6 illustrates the frequency distribution of wind speed differences between SAR-derived observations and the NWP models, MEPS and AROME-Arctic, across various wind regimes. The histograms represent the percentage frequency differences (%) of wind speed occurrences within the valid range of $2 - 25 \text{ m s}^{-1}$ for both models compared to the SAR data, i.e. the frequency of a certain wind speed bin in percent from the SAR data minus the frequency of the same wind speed bin in percent from the model data for all cases in consideration. Note that with this definition the sign of the model bias will be opposite in Figure 6 compared to Table 1.

Both MEPS and AROME-Arctic tend to overestimate the occurrence of lower wind speeds, as indicated by negative frequency differences ranging from approximately -2% to -3% . Specifically, AROME-Arctic exhibits a slightly more pronounced overestimation of the lowest wind speeds compared to MEPS. This consistent bias suggests that both models may struggle to accurately capture wind speeds over a calm sea surface, potentially due to limitations in surface layer parametrization or the representation of stable atmospheric conditions. For moderate wind speeds, both models show a reduction in frequency relative to the SAR-derived observations, with frequency differences exceeding 2% . This indicates a slight underestimation of moderate wind speeds by both MEPS and AROME-Arctic.

As the wind speed increases, corresponding to a rough and very rough sea state, the occur-

rence of such conditions is inherently less frequent. Nevertheless, both models continue to underestimate the frequency of these high wind speeds, as is evident by the positive frequency differences (Figure 6), negative biases, and lower correlation coefficients (Table 1). The limited number of high wind speed instances likely contributes to the poor performance of the models in these conditions, as the small sample size reduces the statistical robustness of the performance metrics. Additionally, the complex non-linear interactions between the wind and waves in these dynamic regimes may pose challenges for the surface layer parametrization of the models.

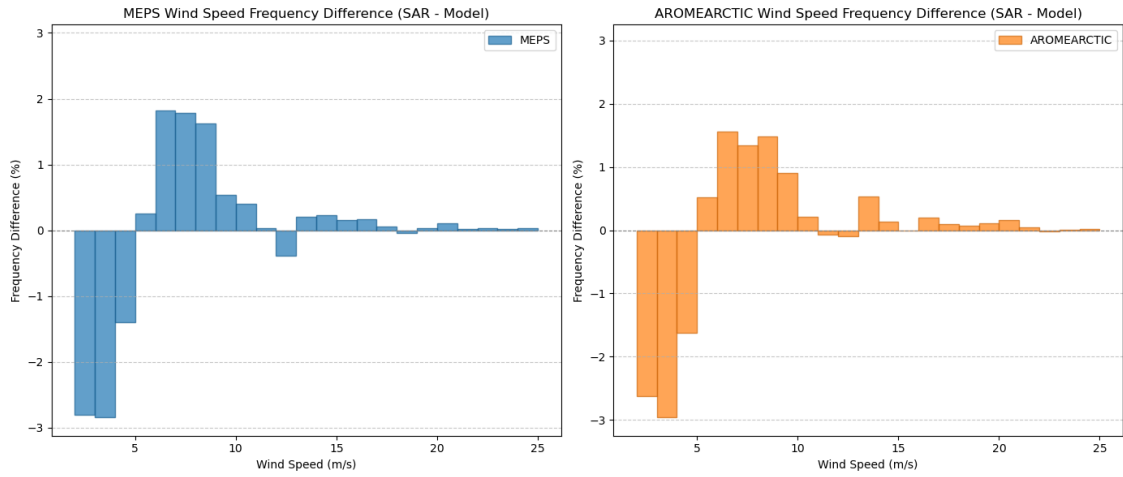


Figure 6: Differences in wind speed occurrence between SAR and MEPS (left), and SAR and AROME-Arctic (right). The frequency of wind speed differences (%) is along the y-axis, and the binned valid wind speeds ($2 - 25 \text{ m s}^{-1}$) are along the x-axis. Both models are within the $\pm 3\%$ range.

3.3 Wind Speed Variability Across Coastal and Open Ocean Regions

In order to further investigate the spatial variability in model performance, the study area is divided into coastal and open ocean regions. Wind dynamics along coastal regions are often more complex due to interactions among orography, thermal gradients, and land-sea surface transitions. Even kilometre-scale models may struggle to accurately capture effects like wind channelling through fjords, and the formation of lee waves.

In open ocean regions, wind patterns tend to be more uniform across large distances, driven primarily by synoptic-scale systems such as high- and low-pressure systems. However, mesoscale disturbances (e.g. polar lows, cold fronts, and convective systems), introduce short-term variability in wind speed and directions. The interaction between the atmosphere and ocean surface in open ocean regions is also modulated by sea surface temperature (SST) gradients and ocean currents, which influence surface winds by modifying pressure gradients and atmospheric stability. These stability conditions may cause challenges for models to accurately represent the associated wind variability, which makes SAR-derived wind fields particularly useful in such cases, as these can capture both the laminar flow under stable conditions and the more turbulent wind structures during unstable conditions.

Geographical Classification of Coastal and Open Ocean Regions

In order to differentiate between 'Coastal' and 'Open Ocean' regions, each data point is geographically classified based on its coordinates relative to a coastal boundary derived from the the Global Self-consistent, Hierarchical, High-resolution Geography Database (GSHHG) coastline shapefile (Wessel et al., 2013). Data points are classified by spatially joining each point's location to this coastal boundary, where points 50 km within these coastal bounds are classified as 'Coastal', while points beyond this distance are labelled as 'Open Ocean'. These boundaries are selected to encompass the Norwegian coastline and surrounding areas in which coastal dynamics are expected to have a significant influence on wind fields. For consistency across models, spatial coordinates are converted from projected coordinates to geographic latitudes and longitudes using the model-specific grid projection.

This classification is applied to the wind field data extracted from the collocated SAR and model data. If a frame is intersected by the boundary between coastal and open ocean, it is

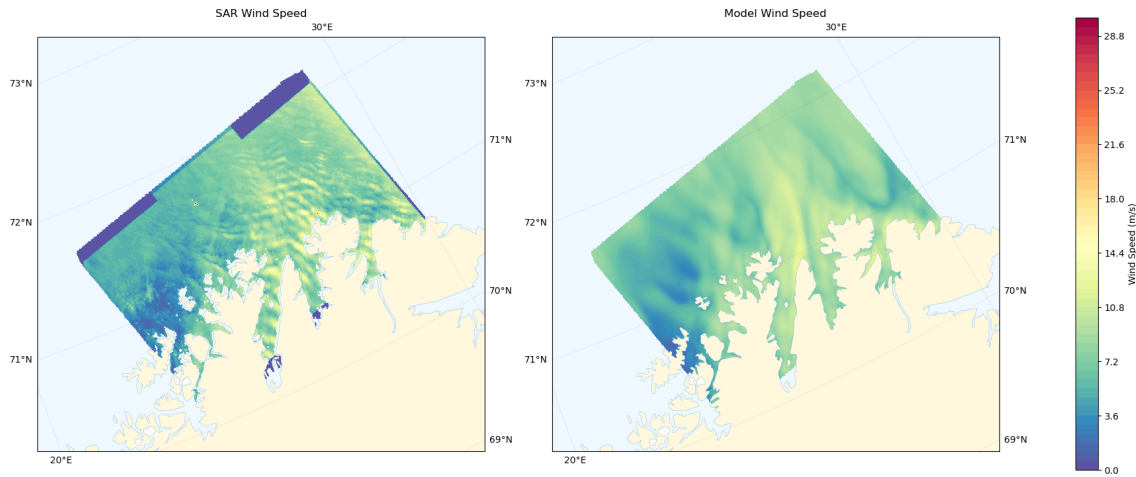
subdivided based on the wind field points within each region, and the resulting subsets are classified accordingly. Once classified, the verification metrics outlined in Section 2.5 are calculated for each individual scene. The final step involves averaging these metrics over the study period, using Fisher's z-transform for averaging correlations across multiple scenes. Classifying wind field points in this manner allows for the quantification of the relative impact of wind dynamics in complex terrain on the NWP models' performance in representing surface winds.

Comparison of Numerical Models and SAR Wind Fields

In order to illustrate the differences in wind field representations between coastal and open ocean regions, sample scenes from both environments are presented. Figure 7 shows wind fields estimated from SAR, AROME-Arctic, and MEPS over the coastal area in the Finnmark region. It is apparent that the striking lee wave pattern in the SAR image is not resolved in the 2.5 km models. It is interesting to see that the signature of the lee waves developed in a stable layer at or above mountain top height is mixed all the way down to sea level, and that the gap winds through the Porsangerfjord and Laksfjord, i.e. the two largest fjords apparent in Figure 7, are superimposed by lee waves. Earlier studies have illuminated that finer spatial resolution than 2.5 km between the grid points is needed in order to resolved lee waves in this area ([Samuelsen and Kvist \(2024\)](#) and [Samuelsen \(2007\)](#))

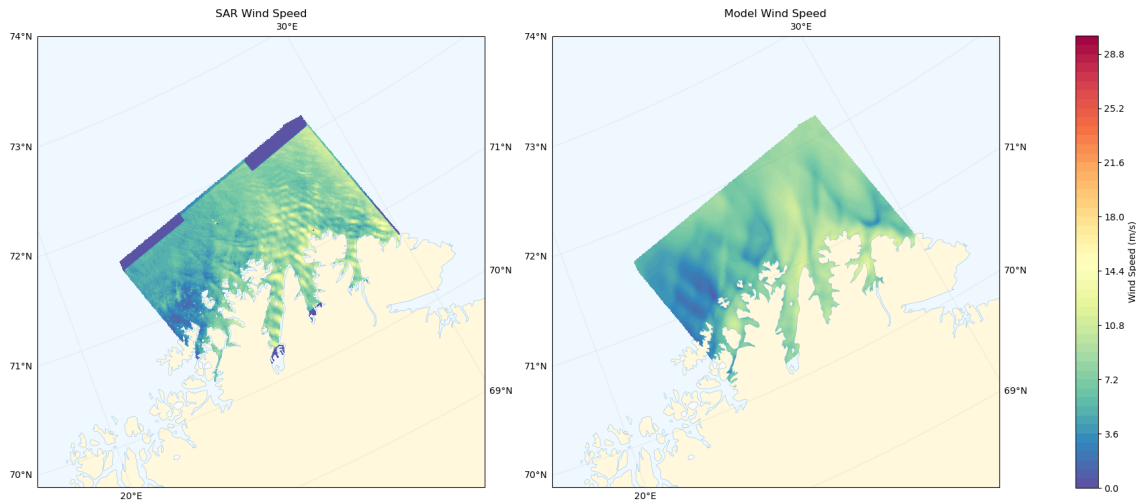
Figure 8 displays corresponding wind fields over an open ocean region in the Norwegian Sea with relatively uniform sea-surface conditions. In this environment, the wind fields from the models exhibit more uniform wind patterns and less spatial variability compared to the coastal region.

Comparison of SAR and Model Wind Speed



(a) MEPS (2024-08-21T15:35:32)

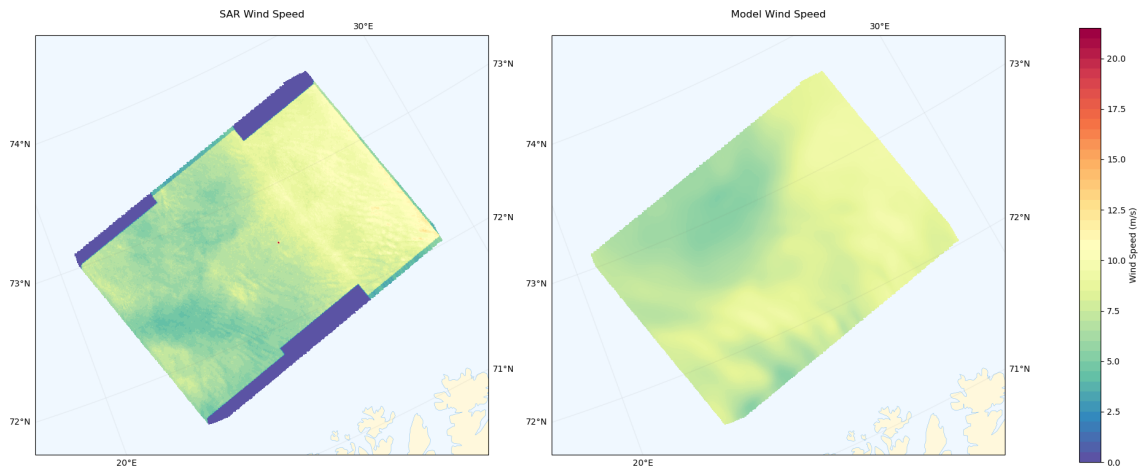
Comparison of SAR and Model Wind Speed



(b) AA (2024-08-21T15:35:32)

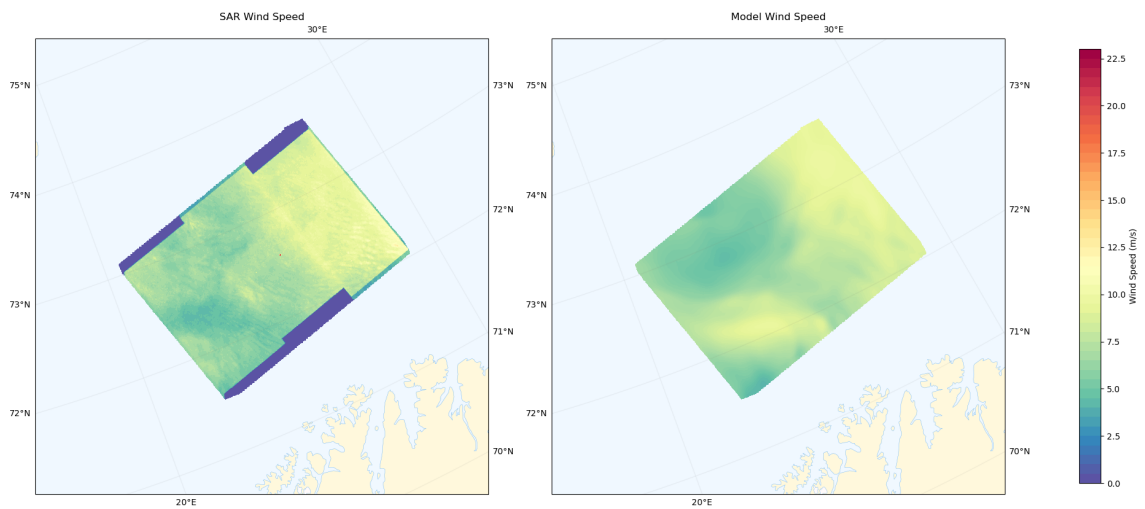
Figure 7: Wind fields compared to SAR over the Finnmark coastline on 21 August 2024, at 15:35:32 UTC, as modelled by (a) MEPS and (b) AROME-Arctic.

Comparison of SAR and Model Wind Speed



(a)

Comparison of SAR and Model Wind Speed



(b)

Figure 8: Wind fields over open water close to the Finnmark coastline 21 August 2024, at 15:35:56 UTC, as modelled by (a) MEPS and (b) AROME-Arctic.

Statistical Comparison Results

The statistical comparison between the numerical models and SAR-derived wind speeds reveals distinct patterns in model performance across coastal and open ocean regions. Table 2 summarizes the averaged verification metrics for both models from the beginning of May 2024 to the end of October 2024, where a total of 238 cases were analysed with MEPS, and 230 cases were analysed with AROME-Arctic.

In *coastal regions*, both AROME-Arctic and MEPS exhibit a negative bias, indicating a systematic underestimation of wind speeds compared to the SAR observations. Specifically, AROME-Arctic has an average bias of -0.98 m s^{-1} , while MEPS shows a slightly larger bias of -1.21 m s^{-1} . The MAE values for the coastal regions are 1.66 m s^{-1} for AROME-Arctic, and 1.75 m s^{-1} for MEPS, which suggests that both models have comparable overall accuracy in predicting wind speeds near the coast. The small difference in MAE suggests that despite AROME-Arctic's smaller bias, both models face similar challenges in reducing absolute errors in the complex coastal environment, likely due to the intricate topography and localized wind phenomena due to the low spatial resolution compared to SAR. The correlation coefficients in coastal regions are relatively low for both models, with AROME-Arctic at 0.28 and MEPS at 0.30. This weak linear relationship between the models and the reference data indicates that the models struggle to capture the full spatial variability of the wind field in these near-shore environments, as observed by the SAR. The slightly higher correlation for MEPS indicates a marginal advantage in representing the variability, but the difference is minimal.

In *open ocean regions*, both models demonstrate improved performance. The biases are smaller, with AROME-Arctic at -0.47 m s^{-1} and MEPS at -0.49 m s^{-1} , indicating a closer agreement with SAR-derived wind speeds. The MAE values are approximately identical for both models at 1.18 m s^{-1} . The higher correlation values for both AROME-Arctic (0.49) and MEPS (0.52) imply that the offshore wind conditions are less challenging for the models to predict, possibly due to less small-scale spatial variability.

Table 2: Averaged verification metrics comparing model-predicted wind speeds from AROME-Arctic and MEPS with SAR-derived wind speeds across coastal and open ocean regions, covering the period from May to October 2024. The table shows the averaged values for bias, MAE, and correlation coefficient, calculated between SAR wind speed and model wind speed for each region and model.

Model	Region	Average Bias (m s^{-1})	Average MAE (m s^{-1})	Average Corr.
MEPS	Coastal	-1.21	1.75	0.30
	Open Ocean	-0.49	1.18	0.52
AROME-Arctic	Coastal	-0.98	1.66	0.28
	Open Ocean	-0.47	1.18	0.49

3.4 Wind Discrepancies in Convective Environments

Convective Event Case Study

Accurate simulation of convective processes is essential, given their crucial role in phenomena such as the genesis and intensification of polar lows. Convection involves the vertical transport of heat and moisture, leading to cloud formation and precipitation, which in NWP simulations are represented through parametrization schemes or explicitly resolved depending on the model resolution. For short-term forecasting of polar lows, AROME-Arctic is operationally used due to its high-resolution capability and regional optimization (Müller et al., 2017). Accuracy in representing convection and boundary layer dynamics in the Arctic is therefore crucial, as it may significantly impact the verification of model forecasts and reliability of predictions for hazardous weather conditions. Due to limited *in-situ* measurements in the region, the presence of sea ice, and shallow planetary boundary layers, further complicates the representation of thermodynamic and dynamic processes that drive polar-low development. The small spatial scales (typically 200-1000 km in diameter) and rapid evolution of polar lows may also challenge model accuracy.

One significant challenge in modeling convection is the *grey-zone* problem (Yu and Lee (2010) and Arakawa and Wu (2013)), where horizontal grid spacings approach scales that partially resolve convective processes, but may still require convection on smaller scales than the effective model resolution. Traditional convection schemes are often not scale-aware and may not perform optimally at these intermediate resolutions. Deciding whether to employ convection parameterization or rely on explicit resolution of convec-

tion can significantly impact the simulation of wind fields, which consequently affects the accurate depiction of polar low structures.

In order to gain a better understanding of these issues, wind field discrepancies between MEPS and AROME-Arctic during two separate convection events are analyzed and compared against the collocated SAR wind observations for the dates 12 October 2024 and 13 October 2024. On 12 October the convection is captured by both MEPS and AROME-Arctic; however, on 13 October, convection is represented by only the MEPS model from the region and time captured by SAR. By examining the structure and intensity of convective cells as captured by the models and observed by SAR, insights may be gained into the limitations of the convective representation of each model and increased awareness around the application of these models as verification during events such as polar lows, sea-spray icing, and hazardous conditions characterized by strong winds and large waves.

Atmospheric Convection in SAR Imagery and NWP Models

Convection involves the formation of updraughts and downdraughts, which creates alternating regions of varying surface roughness on centimetre scales (Sikora et al. (1995) and Ufermann and Romeiser (1999)). Downdraughts enhance near-surface horizontal wind shear by introducing downward-moving, high-momentum airflow. This increased shear amplifies momentum transfer to the sea surface through shear-driven turbulence, resulting in increased radar back-scatter. Conversely, updraughts reduce surface wind shear, leading to decreased surface roughness and lower back-scatter. These interactions cause convection to manifest in SAR imagery as *mottled* (Sikora et al., 1995), characterized by alternating bright and dark regions corresponding to areas of enhanced and diminished surface roughness. As is apparent in Figures 9 and 10, these variations are evident in the SAR-derived wind speed images acquired on 12 October 2024 16:40:56 UTC and on 13 October 2024 06:02:17 UTC. The SAR wind fields for both 12 October and 13 October show wind speeds ranging from around 1.5 m s^{-1} (blue or green regions) up to 25 m s^{-1} (yellow to red regions). The zones with higher wind speeds likely coincide with the descent regions of convective cells, where downdraughts are more intense. In contrast, areas exhibiting lower wind speeds may represent updraught regions within the convective circulation. These convective cells typically occur during cold air outbreaks over warmer sea surfaces, where the thermal contrast creates instability in the marine boundary layer. The sharp transitions between these areas indicate significant wind shear

within the boundary layer, which enhances turbulence and affects the organization and persistence of convective structures.

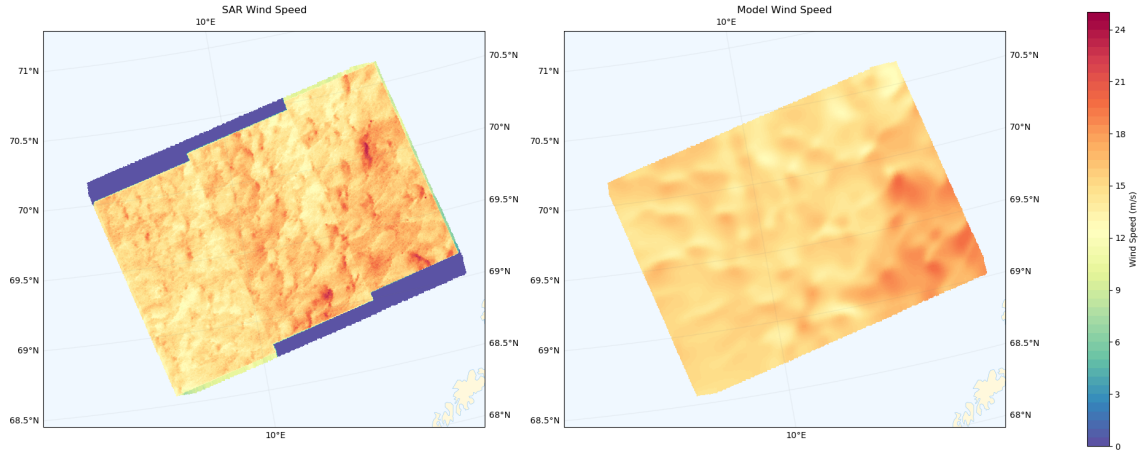
Comparison of NWP Models with SAR Observations

The convective event captured by both MEPS and AROME-Arctic on 12 October shows a well-developed pattern of alternating high and low wind regions. The models broadly capture the extent and morphology of the convective cells, although the estimated wind speeds are slightly lower compared to the SAR observations. Both models underestimate the maximum wind speeds in the core of the convective downdraughts, as well as the sharpness of the wind gradients between adjacent updraught and downdraught regions compared to the SAR-derived wind fields. The maximum wind speed derived from the SAR data on this date for this region and time of day reaches up to 25 m s^{-1} , while MEPS and AROME-Arctic estimate peak winds of around 20 m s^{-1} and 19 m s^{-1} , respectively.

During the convective event on 13 October 2024, MEPS and AROME-Arctic exhibit different responses in their representation of the wind field structures. The MEPS predictions seem to better capture the overall convective patterns that can be observed in the corresponding SAR-derived wind field, with some alternating areas of higher and lower wind speeds. It is important to note, however, the specific structure and magnitude of the convective cells do not align well with the SAR observations. The wind speed gradients are less pronounced in the MEPS model forecast, and the regions of peak wind speeds are shown to be underestimated compared to the SAR data. The maximum wind speed simulated by MEPS is around 17 m s^{-1} , whereas SAR observations indicate values exceeding 23 m s^{-1} in localized areas.

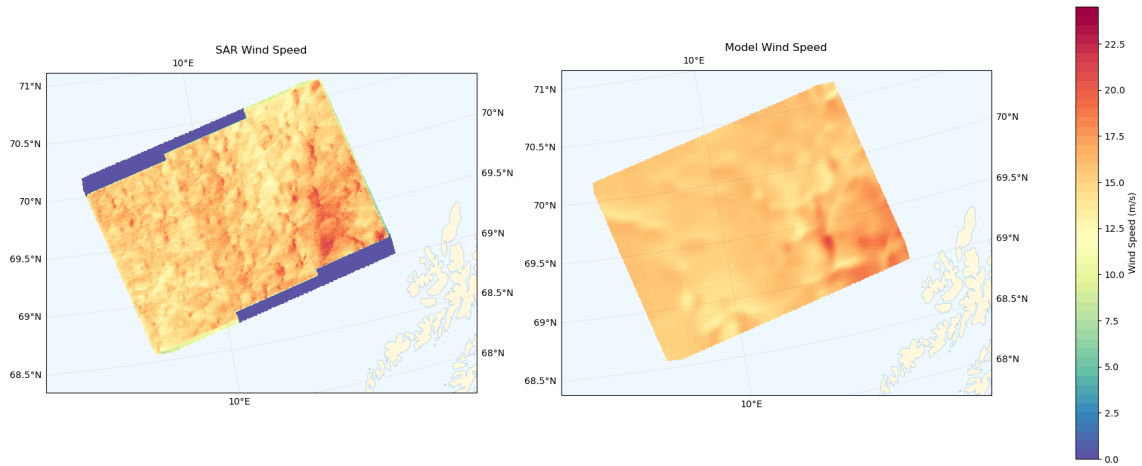
When comparing the AROME-Arctic simulation for the same juncture, this model does not appear to capture any significant convective structures for the region within the SAR swath. A more uniform wind field is observed instead, with a lack of the alternating high and low wind speed patterns characteristic of the observed convective cells. In addition to the lack of resolved convection compared to the MEPS forecast, maximum wind speed values in the AROME-Arctic simulation is still underestimated relative to the SAR wind observations, reaching approximately the same 17 m s^{-1} maximum value as the MEPS forecast.

Comparison of SAR and Model Wind Speed



(a)

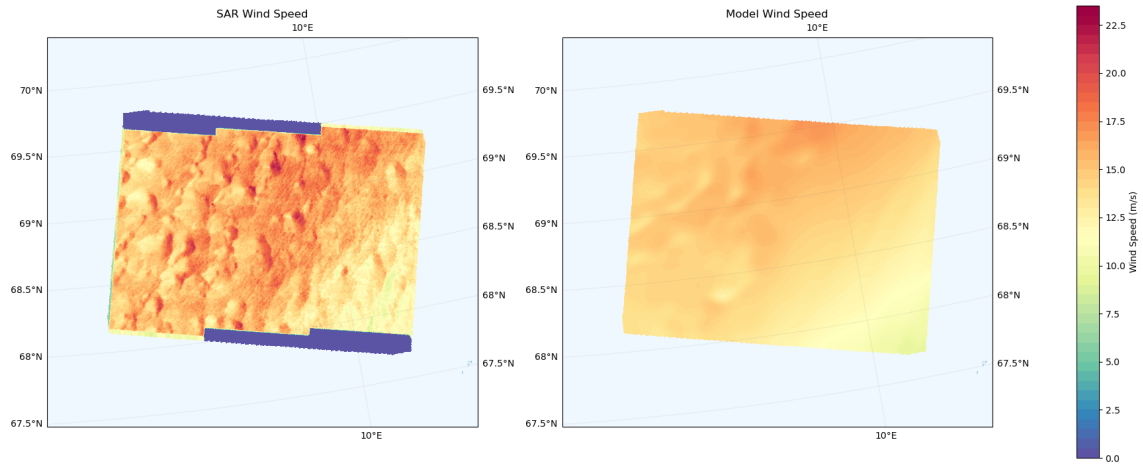
Comparison of SAR and Model Wind Speed



(b)

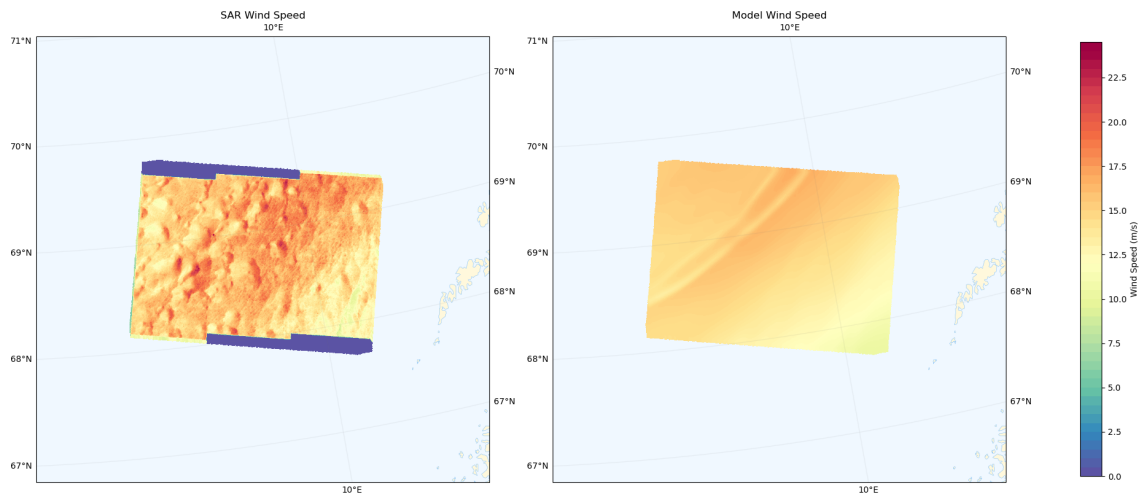
Figure 9: Wind fields during the convective event on 12 October 2024, at 16:40:56 UTC, as modelled by (a) MEPS and (b) AROME-Arctic.

Comparison of SAR and Model Wind Speed



(a)

Comparison of SAR and Model Wind Speed



(b)

Figure 10: Wind fields during the convective event on 13 October 2024, at 06:02:17 UTC, as modelled by (a) MEPS and (b) AROME-Arctic.

The convective event is not only limited to the spatial region captured by the SAR swath on 13 October. However, as simulations from both MEPS and AROME-Arctic indicate organized convective activity persisting further out to the northeast and northwest of the SAR frame (not shown). Observed differences in the model representation of these events show the system moving in from the south of the SAR frame is already well-developed in the broader domain of the MEPS forecast, but is largely absent in the AROME-Arctic simulation for the same time period, closer to the lower boundary of the AROME-Arctic model domain.

4 Discussion

The evaluation of NWP models against SAR-derived wind fields highlights several challenges and limitations that impact the accuracy of operational wind field verification, particularly in high-latitude environments. SAR wind data, especially when employing the EW swath mode and HH polarization, are susceptible to ambiguities introduced by sea-ice dynamics in Arctic regions. Variations in backscatter caused by sea-ice drift and the misclassification of ice-related roughness as high wind speeds lead to systematic overestimation in ice-covered areas. The discrepancies result in poor correlation between SAR-derived winds and NWP model outputs, suggesting that integrating SAR wind products with NWP models using these swaths should be approached with caution.

Advancements in SAR wind retrieval algorithms offer potential solutions to these limitations. For instance, cross-polarization (HV or VH) has demonstrated improved capabilities in distinguishing between sea ice and open water, potentially reducing misclassification errors in wind speed retrievals (Zhao et al., 2024). Additionally, the use of dual co-polarized SAR configurations, such as VV, HH, and VV/VH ratio, has been suggested to enhance operational utility (Geldsetzer and Yackel, 2009). Advanced retrieval algorithms, including neural network-based approaches and Support Vector Machine (SVM) methods, have shown promise in enhancing the performance of SAR-based wind field derivation in the presence of drift ice. For instance, an SVM-based sea ice discrimination method applied to Sentinel-1 EW mode data achieved a matching rate of approximately 93.4% when validated against manually classified ice maps (Hong and Yang, 2018), demonstrating potential for operational use.

The comparative analysis of MEPS and AROME-Arctic against SAR-derived wind fields elucidates common performance deficiencies linked to sea-surface conditions. Both models exhibit a tendency to overestimate wind speeds under calm conditions, and underestimate them in rough and very rough sea states. This pattern suggests that the models might struggle to accurately represent the complex interaction between the atmospheric boundary layer, which is a known challenge in high-latitude regions where stable conditions suppress turbulence and vertical mixing (Mahrt, 2011). Limitations in turbulence and parametrization schemes may lead to overestimation of wind speeds in calm conditions. On the other hand, underestimation in rough conditions may result from inadequate

adjustment of surface drag coefficient. [Donelan et al. \(2004\)](#) point to the fact that in rough conditions the sea surface is characterized by large waves, whitecaps, and increased foam coverage, which enhance surface roughness and, consequently, the momentum transfer between the atmosphere and ocean. If the models do not adequately adjust the surface drag coefficient to account for these changes, the models may underestimate the frictional forces, leading to higher simulated wind speeds near the surface. However, in this situation the models are in fact underestimating the strong winds, meaning that there must be other explanations involved. As already mentioned the challenge in resolving features like showers and lee waves in the models may be an explanation for the systematic underestimation of strong winds in this area.

Correlation coefficients between model forecasts and SAR-derived wind speeds provide further insights into model performance. Both the MEPS and AROME-Arctic models achieve higher correlations under moderate sea surface conditions (Table 1), indicating better skill in capturing spatial variability when conditions are neither too calm nor too extreme. However, in high wind conditions, models not only underestimate wind speeds but also struggle to capture the temporal and spatial variability inherent in such events which may also be explained by the challenge in resolving convective cells and lee waves in an accurate manner. The consistent patterns observed across different models imply that these deficiencies may be inherent to the Arome 2.5 km models applied in the current study.

In coastal regions, both MEPS and AROME-Arctic display a tendency to underestimate wind speeds, even more so along the coastal regions compared to open ocean areas. In regions of complex terrain, MEPS underestimates wind speeds more significantly than AROME-Arctic on average, as seen in Table 2. The ability to capture spatial variability is comparable between the two models, with both exhibiting relatively weak correlations in areas affected by complex topography. Due to the enhanced small-scale fluxes in these zones, the grid-based approach of NWP models often struggles to fully resolve the fine-scale wind features ([Draxl et al., 2014](#)).

Both models show improved performance in open ocean areas farther from the coastline, where wind patterns are less affected by terrain-induced wind flows. Despite the increased accuracy over open ocean compared to coastal complex terrain, the correlation

coefficients of the models suggest that there is still room for enhancement in capturing the temporal and spatial variability of open ocean winds, which may be due to the models' limitations in resolving transient weather systems and small-scale phenomena that can significantly impact wind speeds and direction. Furthermore, the representation of marine boundary layer processes can differ significantly from land-based dynamics, and if the models' parametrizations are not fully optimized for oceanic conditions, this could contribute to the observed discrepancies. For operational forecasting, this level of correlation may be acceptable in scenarios where general trends are more important than accurate precision.

In addition to these challenges, the interpretation of SAR-derived winds is complicated by an under-determination problem ([Portabella et al., 2002](#)). A single Normalized Radar Cross Section (NRCS) measurement is sensitive to both wind speed and direction, and multiple combinations of these variables can produce the same NRCS response. This means that without precise wind direction information, it is difficult to accurately distinguish wind speed from direction based on NRCS data alone. Therefore, any inaccuracies in the wind direction input from the model may lead to ambiguities in the retrieved wind speed, as the under-determination problem makes it impossible to fully isolate the effects of wind speed and direction.

5 Conclusions

This study assesses the performance of two high-resolution Numerical Weather Prediction (NWP) models, MEPS and AROME-Arctic, by comparing their 10-m wind predictions with Synthetic Aperture Radar (SAR)-derived wind fields across the European Arctic from the beginning of May 2024 to the end of October 2024. The research is driven by the need for improved atmospheric modelling in the Arctic, a region where sparse observational networks and unique meteorological phenomena such as polar lows challenge forecasting accuracy. SAR data offer high-resolution insights into surface wind fields, providing fine-scale spatial and temporal variability that operational NWP models lack.

Key findings indicate that both MEPS and AROME-Arctic models show systematic biases. In calm sea conditions, both models tend to overestimate wind speeds, likely due to limitations in surface layer parametrizations under stable atmospheric conditions. Conversely, under rough and very rough sea states, both models consistently underestimate wind speeds, highlighting challenges in resolving high-wind scenarios influenced by non-linear wind-wave interactions. The analysis further reveals that model performance improves in open ocean regions, where wind dynamics are more uniform and less influenced by coastal orographic effects. However, both models struggle to accurately capture wind variability and gradients in complex coastal terrains.

A case study of a convective system is briefly investigated, where the models exhibit significant discrepancies in predicting the structure and intensity of convective cells. Case studies on 12 and 13 October 2024, reveal underestimations of peak wind speeds and subdued representation of convective patterns compared to SAR-derived observations. AROME-Arctic, in particular, shows challenges in representing organized convective activity, underscoring the need for improved resolution and convection schemes in NWP models for Arctic weather systems.

The study also highlights the inherent limitations of SAR data, such as ambiguities introduced by sea ice dynamics. Misclassification of ice-related roughness as high wind speeds reduces the reliability of SAR-derived data in ice-covered areas, emphasizing the need for advanced retrieval algorithms.

Nevertheless, as long as one is aware of the aforementioned limitations of the SAR data, the potential value of using SAR-data for model verification over observation sparse ocean areas is clearly highlighted. The advantage of the SAR data is particularly apparent in conjunction with weather phenomena with large spatial variations in wind field with a signature over the ocean like convective situations and lee waves. This also shows the potential benefit of using SAR data as input to nowcasting wind products instead of modelled wind speed for moderate or strong wind events like ship-icing events ([Samuelsen, 2018](#)). In order to follow this up further, models with higher resolution than the operational models should be compared with SAR data for various cases.

Acknowledgements

The authors wish to acknowledge Frode Dinessen for his guidance and role in providing the SAR wind data. Gratitude goes to the Research Council of Norway for the financial support through the project “Multidisciplinary approach for spray icing modelling and decision support in the Norwegian maritime sector” (SPRICE). This project is funded under the MAROFF-2 Programme [Grant Number: 320843].

References

- Arakawa, A. and Wu, C.-M. (2013). A Unified Representation of Deep Moist Convection in Numerical Modeling of the Atmosphere. Part I. *Journal of the Atmospheric Sciences*, 70(7):1977 – 1992.
- Bengtsson, L., Andrae, U., Aspelién, T., Batrak, Y., Calvo, J., de Rooy, W., Gleeson, E., Hansen-Sass, B., Homleid, M., Hortal, M., Ivarsson, K.-I., Lenderink, G., Niemelä, S., Nielsen, K. P., Onvlee, J., Rontu, L., Samuelsson, P., Muñoz, D. S., Subias, A., Tilm, S., Toll, V., Yang, X., and Køltzow, M. Ø. (2017). The HARMONIE–AROME Model Configuration in the ALADIN–HIRLAM NWP System. *Monthly Weather Review*, 145(5):1919–1935.
- Donelan, M. A., Haus, B. K., Reul, N., Plant, W. J., Stiassnie, M., Graber, H. C., Brown, O. B., and Saltzman, E. S. (2004). On the limiting aerodynamic roughness of the ocean in very strong winds. *Geophysical Research Letters*, 31(18).
- Draxl, C., Hahmann, A. N., Peña, A., and Giebel, G. (2014). Evaluating winds and vertical wind shear from Weather Research and Forecasting model forecasts using seven planetary boundary layer schemes. *Wind Energy*, 17(1):39–55.
- Elvidge, A. D., Renfrew, I. A., Weiss, A. I., Brooks, I. M., Lachlan-Cope, T. A., and King, J. C. (2016). Observations of surface momentum exchange over the marginal ice zone and recommendations for its parametrisation. *Atmos. Chem. Phys.*, 16:1545–1563.
- Geldsetzer, T. and Yackel, J. J. (2009). Sea ice type and open water discrimination using dual co-polarized C-band SAR. *Canadian Journal of Remote Sensing*, 35(1):73–84.
- Hersbach, H., Stoffelen, A., and de Haan, S. (2007). An improved C-band scatterometer ocean geophysical model function: CMOD5. *Journal of Geophysical Research: Oceans*, 112(C3).
- Hong, D.-B. and Yang, C.-S. (2018). Automatic discrimination approach of sea ice in the Arctic Ocean using Sentinel-1 Extra Wide Swath dual-polarized SAR data. *International Journal of Remote Sensing*, 39(13):4469–4483.
- Horstmann, J., Koch, W., Lehner, S., and Tonboe, R. (2000). Wind retrieval over the

- ocean using synthetic aperture radar with C-band HH polarization. *IEEE Transactions on Geoscience and Remote Sensing*, 38(5):2122–2131.
- Huber, P. (2004). *Robust Statistics*. Wiley Series in Probability and Statistics - Applied Probability and Statistics Section Series. Wiley.
- Johannessen, O. M. (2020). Annex: SAR Sea Ice Interpretation Guide. In Johannessen, O. M., Bobylev, L. P., Shalina, E. V., and Sandven, S., editors, *Sea Ice in the Arctic: Past, Present and Future*, pages 507–573. Springer International Publishing, Cham.
- Jung, T. and Leutbecher, M. (2007). Performance of the ECMWF forecasting system in the Arctic during winter. *Quarterly Journal of the Royal Meteorological Society*, 133(626):1327–1340.
- Jung, T. and Matsueda, M. (2016). Verification of global numerical weather forecasting systems in polar regions using TIGGE data. *Quarterly Journal of the Royal Meteorological Society*, 142(695):574–582.
- Køltzow, M., Grote, R., and Singleton, A. (2021). On the configuration of a regional Arctic Numerical Weather Prediction system to maximize predictive capacity. *Tellus A: Dynamic Meteorology and Oceanography*, 73(1):1–18.
- Køltzow, M., Øiestad, M., Azad, R., Rugaard Furevik, B., Olsen, A.-M., and Remes, T. (2024). How inaccurate offshore wind observations impact the quality of operational numerical weather prediction. *Quarterly Journal of the Royal Meteorological Society*, 150(765):5337–5355.
- Mahrt, L. (2011). The Near-Calm Stable Boundary Layer. *Boundary-Layer Meteorology*, 140:343–360.
- Müller, M., Batrak, Y., Kristiansen, J., Køltzow, M. A. Ø., Noer, G., and Korosov, A. (2017). Characteristics of a Convective-Scale Weather Forecasting System for the European Arctic. *Monthly Weather Review*, 145(12):4771–4787.
- Olsen, A.-M., Øiestad, M., Berge, E., Køltzow, M. , and Valkonen, T. (2022). Evaluation of Marine Wind Profiles in the North Sea and Norwegian Sea Based on Measurements and Satellite-Derived Wind Products. *Tellus A: Dynamic Meteorology and Oceanography*.

- Onstott, R. G. (1992). SAR and Scatterometer Signatures of Sea Ice. In *Microwave Remote Sensing of Sea Ice*, chapter 5, pages 73–104. American Geophysical Union (AGU).
- Portabella, M., Stoffelen, A., and Johannessen, J. A. (2002). Toward an optimal inversion method for synthetic aperture radar wind retrieval. *Journal of Geophysical Research: Oceans*, 107(C8):1–13.
- Rousseeuw, P. J. and Croux, C. (1993). Alternatives to the Median Absolute Deviation. *Journal of the American Statistical Association*, 88(424):1273–1283.
- Samuelsen, E. M. (2007). Et dynamisk studium av stormen Narve - et kaldluftsutbrudd i Finnmark - ved hjelp av observasjoner og numeriske simuleringer. (A dynamical study of the storm Narve - a cold air outbreak in Finnmark - with the use of observations and numerical simulations.). Master's thesis, University of Bergen, Bergen. [Available online at <http://hdl.handle.net/1956/17137>. Accessed 05 March 2018.].
- Samuelsen, E. M. (2018). Ship-icing prediction methods applied in operational weather forecasting. *Quarterly Journal of the Royal Meteorological Society*, 144(710):13–33.
- Samuelsen, E. M. and Kvist, K. (2024). Icing Observed and Analysed in Correspondence with Helicopter Flight Campaigns in Norway in 2023. In Virk, M. S., editor, *20th International Workshop on Atmospheric Icing of Structures (IWAIS 2024) Conference Proceedings*, pages 51–56. UiT - The Arctic University of Norway.
- Sikora, T., Young, G., Beal, R., and Edson, J. (1995). Use of spaceborne synthetic aperture radar imagery of the sea surface in detecting the presence and structure of the convective marine atmospheric boundary layer. *Monthly Weather Review*, 123(12):3623–3632.
- Solbrekke, I. M., Sorteberg, A., and Haakenstad, H. (2021). The 3 km Norwegian re-analysis (NORA3) – a validation of offshore wind resources in the North Sea and the Norwegian Sea. *Wind Energy Science*, 6(6):1501–1519.
- Stoffelen, A., Verspeek, J. A., Vogelzang, J., and Verhoef, A. (2017). The cmod7 geophysical model function for ascats and ers wind retrievals. *IEEE Journal of Selected Topics in Applied Earth Observations and Remote Sensing*, 10(5):2123–2134.

- Tollinger, M., Graversen, R., and Johnsen, H. (2021). High-resolution polar low winds obtained from unsupervised SAR wind retrieval. *Remote Sensing*, 13(22):4655.
- Tollinger, M. and Graversen, R. G. (2024). Validation of a SAR-Only Wind-Vector Retrieval Against Shipborne In Situ Wind Observations in the European Arctic. *IEEE Transactions on Geoscience and Remote Sensing*, 62:1–11.
- Ufermann, S. and Romeiser, R. (1999). Numerical study on signatures of atmospheric convective cells in radar images of the ocean. *Journal of Geophysical Research: Oceans*, 104(C11):25707–25719.
- Wessel, P., Smith, W. H. F., Scharroo, R., Luis, J., and Wobbe, F. (2013). Generic Mapping Tools: Improved Version Released. *Eos, Transactions American Geophysical Union*, 94(45):409–410.
- Wu, L., ø. Breivik, and Rutgersson, A. (2019). Ocean-wave-atmosphere interaction processes in a fully coupled modeling system. *J. Adv. Model. Earth Syst.*, 11:3852–3874.
- Yu, X. and Lee, T.-Y. (2010). Role of convective parameterization in simulations of a convection band at grey-zone resolutions. *Tellus A: Dynamic Meteorology and Oceanography*, 62(5):617–632.
- Zhao, L., Xie, T., Perrie, W., and Yang, J. (2024). Sea Ice Detection from RADARSAT-2 Quad-Polarization SAR Imagery Based on Co- and Cross-Polarization Ratio. *Remote Sensing*, 16(3).